UC San Diego

UC San Diego Previously Published Works

Title

Microbial DNA enrichment promotes liver steatosis and fibrosis in the course of non-alcoholic steatohepatitis

Permalink

https://escholarship.org/uc/item/8xn67729

Journal

Acta Physiologica, 235(3)

ISSN

1748-1708

Authors

Luo, Zhenlong
Ji, Yudong
Zhang, Dinghong
et al.

Publication Date

2022-07-01

DOI

10.1111/apha.13827

Peer reviewed

eScholarship.org Powered by the California Digital Library
University of California

Check for updates

Received: 10 March 2022 | Revised: 27 April 2022 | Accepted: 29 April 2022

DOI: 10.1111/apha.13827

ACTA PHYSIOLOGICA

REGULAR PAPER

Microbial DNA enrichment promotes liver steatosis and fibrosis in the course of non-alcoholic steatohepatitis

Zhenlong Luo[1,2] | **Yudong Ji**[1,3] | **Dinghong Zhang**[1] | **Hong Gao**[1] | **Zhongmou Jin**[4] | **Meixiang Yang**[5,6] | **Wei Ying**[1]

[1]Division of Endocrinology & Metabolism, Department of Medicine, University of California, San Diego, California, USA

[2]Department of Gastroenterology, Tongji Hospital, Tongji Medical College, Huazhong University of Science and Technology, Wuhan, China

[3]Department of Anesthesiology, Institute of Anesthesiology and Critical Care, Union Hospital, Tongji Medical College, Huazhong University of Science and Technology, Wuhan, China

[4]Division of Biological Sciences, University of California, San Diego, California, USA

[5]Pediatric Diabetes Research Center, Department of Pediatrics, University of California, San Diego, California, USA

[6]Zhuhai Institute of Translational Medicine, Zhuhai People's Hospital Affiliated with Jinan University, Biomedical Translational Research Institute, Jinan University, Guangzhou, China

Correspondence
Wei Ying, Division of Endocrinology & Metabolism, Department of Medicine, University of California, San Diego, CA, USA.
Email: weying@health.ucsd.edu

Funding information
National Institute of Diabetes and Digestive and Kidney Diseases, Grant/Award Number: R00DK115998 and R01DK125560; UCSD School of Medicine Microscopy Core, Grant/Award Number: P30 NS047101; National Natural Science Foundation of China, Grant/Award Number: 81500436; UCSD/UCLA Diabetes Research Center Pilot and Feasibility, Grant/Award Number: P30 DK063491

Abstract

Aim: Low-grade inflammation is the hallmark of non-alcoholic fatty liver diseases (NAFLD) and non-alcoholic steatohepatitis (NASH). The leakage of microbiota-derived products can contribute to liver inflammation during NAFLD/NASH development. Here, we assessed the roles of gut microbial DNA-containing extracellular vesicles (mEVs) in regulating liver cellular abnormalities in the course of NAFLD/NASH.

Methods: We performed studies with Vsig4$^{-/-}$, C3$^{-/-}$, cGAS$^{-/-}$, and their wild-type littermate mice. Vsig4+ macrophage population and bacterial DNA abundance were examined in both mouse and human liver by either flow cytometric or immunohistochemistry analysis. Gut mEVs were adoptively transferred into Vsig4$^{-/-}$, C3$^{-/-}$, cGAS$^{-/-}$, or littermate WT mice, and hepatocyte inflammation and HSC fibrogenic activation were measured in these mice.

Results: Non-alcoholic fatty liver diseases and non-alcoholic steatohepatitis development was concomitant with a diminished liver Vsig4+ macrophage population and a marked bacterial DNA enrichment in both hepatocytes and HSCs. In the absence of Vsig4+ macrophages, gut mEVs translocation led to microbial DNA accumulation in hepatocytes and HSCs, resulting elevated hepatocyte inflammation and HSC fibrogenic activation. In contrast, in lean WT mice, Vsig4+ macrophages remove gut mEVs from bloodstream through a C3-dependent opsonization mechanism and prevent the infiltration of gut mEVs into hepatic cells. Additionally, Vsig4$^{-/-}$ mice more quickly developed significant liver steatosis

Zhenlong Luo, Yudong Ji and Dinghong Zhang contributed equally.

© 2022 Scandinavian Physiological Society. Published by John Wiley & Sons Ltd

and fibrosis than WT mice after Western diet feeding. In vitro treatment with NASH mEVs triggered hepatocyte inflammation and HSC fibrogenic activation. Microbial DNAs are key cargo for the effects of gut mEVs by activating cGAS/STING.

Conclusion: Accumulation of microbial DNAs fuels the development of NAFLD/NASH-associated liver abnormalities.

KEYWORDS

liver fibrogenic activation, liver inflammation, microbial DNAs, microbiota-derived extracellular vesicles, Vsig4+ macrophages

1 | INTRODUCTION

The ongoing metabolic syndrome and diabetes epidemic are driving a parallel rise in the prevalence of non-alcoholic fatty liver diseases (NAFLD) and non-alcoholic steatohepatitis (NASH).[1–3] It has become clear that chronic and subacute liver inflammation can fuel the development of NAFLD and subsequent transition to NASH.[4–6] Emerging evidence reveals that chronic inflammation triggers cellular abnormalities in hepatocytes and hepatic stellate cells (HSCs), both of which contribute to the incidence of NAFLD and NASH.[4–6] The origins of liver inflammation include lipotoxicity,[7–10] bile acids,[11–13] innate immune responses,[14–16] hepatocellular stress, and death.[17–20]

Overweight is accompanied by gut barrier breach, which leads to the leakage of microbiota-derived products into host circulation and distant organs.[21–25] Changes in microbiota composition and function occur in response to the pathogenesis of metabolic diseases.[26] Emerging evidence indicates the critical roles of microbial metabolites in the incidence of tissue inflammation and metabolic abnormalities.[27–32] Besides, several reports have shown the enrichment of microbial DNAs in the bloodstream and various metabolic organs of both obese humans and mice.[33–37] In addition, these circulating microbial DNAs could serve as biomarkers mirroring the states of metabolic diseases.[33,36,38] It has been known that extracellular vesicles (EVs) play critical roles in cellular transportation of a variety of cargoes, including nucleic acids, proteins, and lipids.[39] A wide range of microbiota species secrete EVs which may play important roles in communicating with microbiota or host cells.[40,41] However, whether microbiota-derived bacterial DNA-containing EVs could be translocated from gut lumen into host circulation and affect the inflammatory responses in hepatic cells during NASH development remains to be clarified.

Live immune alteration is also a factor that can change the action of bacterial translocation in NAFLD/NASH. Previous studies have demonstrated that Vsig4 (V-set and immunoglobulin domain containing 4) expression is required for the ability of Kupffer cells to remove complement C3-opsonized products.[42,43] Our previous findings have revealed that the expression of Vsig4 is remarkably decreased in Kupffer cells in the liver of obese mice and Vsig4+ Kupffer cells play an important role in clearing microbiota-derived EVs from bloodstream.[43] However, the important roles of Vsig4+ Kupffer cells in the pathogenesis of NAFLD/NASH is largely unknown.

Here, we report that microbial DNA accumulation is a pathogenic factor driving cellular abnormalities in hepatocytes and HSCs during the development of NAFLD/NASH. We found a marked accumulation of bacterial DNAs within hepatocytes and HSCs in both NAFLD/NASH human and mouse liver. In the course of NASH Vsig4+, liver macrophage population was diminished, resulting in the penetration of gut mEVs into both hepatocytes and HSCs. We further validated that microbial DNAs are key cargoes within gut EVs triggering hepatic cellular abnormalities through the activation of cGAS/STING signaling.

2 | RESULTS

2.1 | Bacterial DNAs are accumulated in HSCs in the context of NASH

We first assessed the abundance of bacterial DNAs in mouse liver after 24 weeks Western diet feeding (NASH; Figure S1A). As shown in Figure 1(A), robust 16s rRNA signals were detected in the hepatic α-smooth muscle actin+ (α-SMA+) cells of NASH WT mice, whereas much less abundance of bacterial DNAs was observed in lean WT mouse liver. We also found that NAFLD/NASH human HSCs contained greater amount of bacterial DNAs than that in normal healthy human liver (Figure 1B; Table S1). To assess the impact of external bacterial DNA contamination during these experiments,

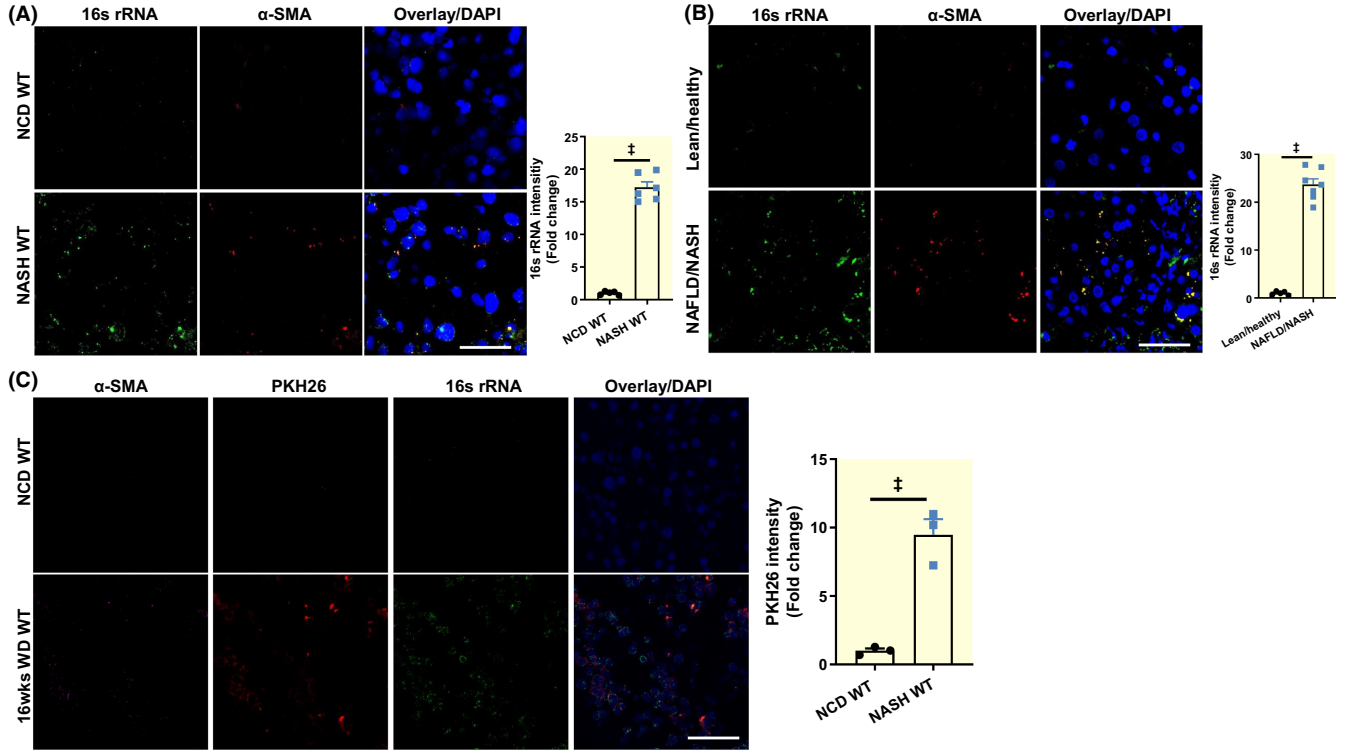

FIGURE 1 Bacterial DNAs are enriched in hepatic stellate cells (HSCs) in the context of NAFLD/NASH. The abundance of 16s rRNA in the hepatic α-SMA+ cells of NCD or 24 weeks western diet-fed (24-week WD; NASH) WT mice (a), healthy lean or NAFLD/NASH human liver (B). (C) The levels of PKH26 red fluorescence and 16s rRNA in hepatic α-SMA+ cells after injection of PKH26-labeled intestinal EVs into the jejunum sections of both NCD and 16-week WD-fed WT mice. Data are the representative of three experiments and the images were from the area closed to portal vein zonation of livers (A–C). (A–C) Scale bar = 50 μm. ‡$p < 0.001$, Student's *t* test.

we also detected 16s rRNA signals in the liver of germ-free mice. We found no bacterial DNA signal in these germ-free liver samples (Figure S1B), thus confirming minimal exogenous bacterial DNA contamination in our experiments.

Non-alcoholic steatohepatitis development is accompanied by the impaired gut barrier (Figure S1C), and our previous study has shown that microbial DNA-containing intestinal extracellular vesicles (mEVs) are readily translocated from gut lumen into host circulation and liver in the context of obesity.[43,44] We also detected bacterial DNA in the plasma EVs isolated from WD-fed WT mice, whereas very few number of bacterial DNA was detected in lean mouse plasma EVs (Figure S1D). Thus, we next tested if mEVs pass through gut barrier and deliver microbial DNAs into HSCs in both lean and NASH WT mice. Using our previously reported mEV isolation method, mEVs were collected from the small intestinal lumen of 16-week Western diet-fed WT mice and then labeled with PKH26 red fluorescent dye (Figure 1C and Figure S1E,F). After 16 h injection of PKH26 mEVs into the jejunum section of 16-week Western diet-fed WT recipient mice, we observed strong red fluorescent signals presented in hepatic α-SMA+ cells (Figure 1C). In contrast, much fewer PKH26 signals were detected in the liver of lean WT mice (Figure 1C). Taken together, these data indicate that the impaired gut barrier allows for the translocation of intestinal mEVs and accumulation of microbial DNAs in NASH HSCs.

2.2 | Loss of hepatic Vsig4+ macrophages leads to infiltration of gut mEVs into HSCs

Liver Vsig4+ macrophages are main effector cells removing bacterial products from bloodstream. However, the proportion of Vsig4+F4/80+ cells was significantly decreased after 24-week Western diet feeding, compared to lean WT mice (Figure 2A,B). To demonstrate the importance of Vsig4+ cells on blocking translocation of gut mEVs into HSCs and hepatocytes, NASH gut mEVs were intravenously injected into either lean WT or Vsig4$^{-/-}$ mice (1×10^{10} EVs/mouse, twice injection per week). After 4-week injection, qPCR analysis indicates a marked increase in 16s rRNA abundance in both HSCs and hepatocytes isolated from NCD Vsig4$^{-/-}$-recipient mice, whereas there were barely detectable bacterial DNAs in the HSCs and hepatocytes collected from NCD

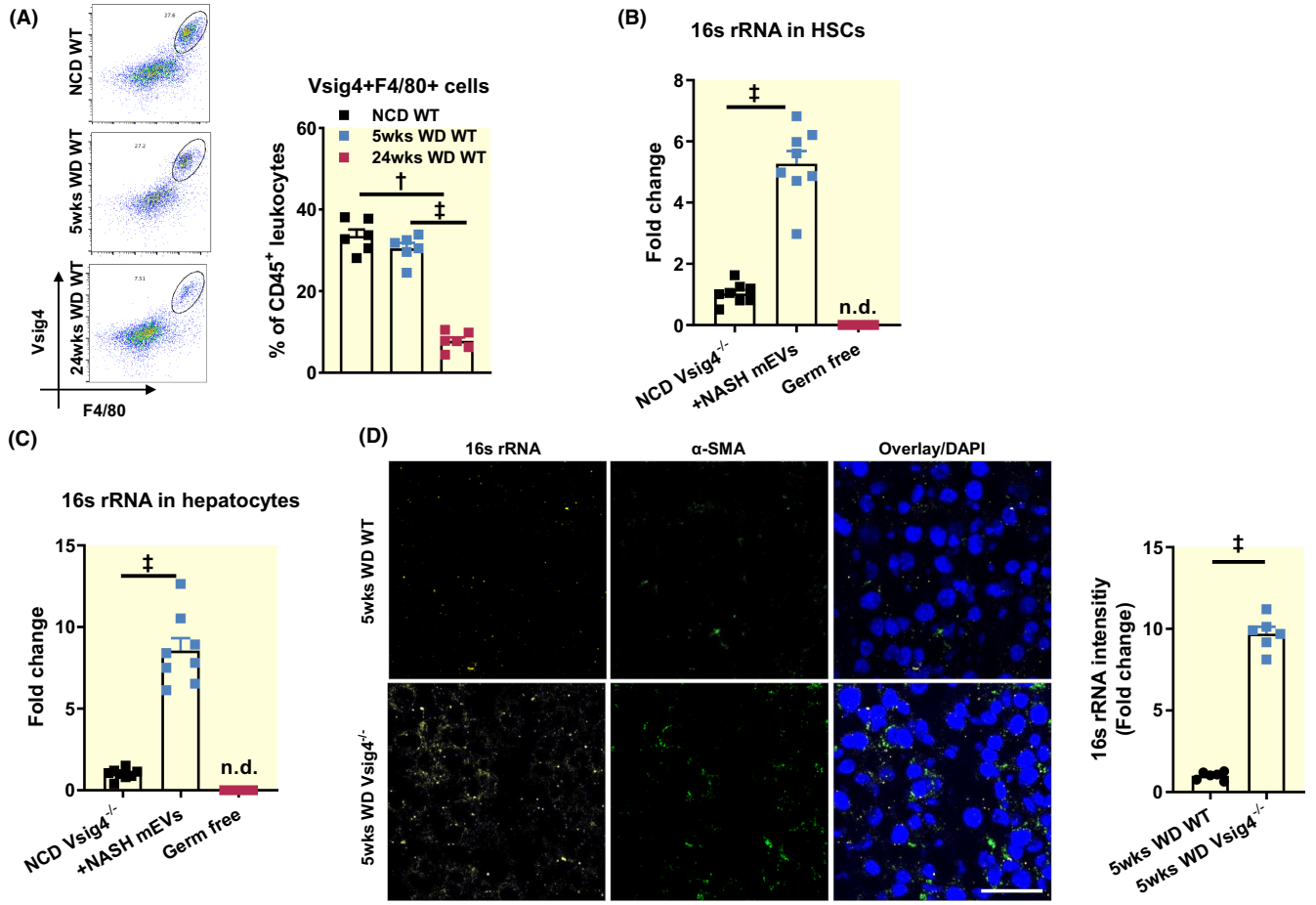

FIGURE 2 Vsig4+ macrophages block the translocation of gut mEVs into HSCs. (A) Flow cytometric analysis of liver Vsig4+ macrophage population in NCD and Western diet (WD)-fed WT mice. qPCR analysis of 16s rRNA abundance in the HSCs (B) and hepatocytes (C) of NCD germ-free mice or NCD Vsig4$^{-/-}$ mice treated with 4-week NASH gut mEVs. (D) The abundance of 16s rRNA in the hepatic α-SMA+ cells of 5-week Western diet-fed WT and Vsig4$^{-/-}$ mice. Data are presented as mean ± SEM. (D) Scale bar = 50 μm; data are the representative of three experiments. †$p < 0.01$, ‡$p < 0.001$, Student's t test. mEV, microbial DNA-containing extracellular vesicles. n.d., non-detectable.

WT recipients (Figure 2B,C). Hepatic cells were also isolated from germ-free mice with the same protocol and used benchmark controls to evaluate the contamination of environmental bacterial DNAs. Bacterial DNA was not detectable from these germ-free hepatic cells, thus demonstrating the minimal level of external bacterial DNA contamination in our experiments (Figure 2B,C).

We also observed that a short-term (5 weeks) Western diet feeding did not significantly change the population of liver Vsig4+F4/80+ cells (Figure 2A), preventing accumulation of microbial DNAs in HSCs and hepatocytes. However, 5-week Western diet-fed Vsig4$^{-/-}$ mice displayed a greater amount of 16s rRNAs in the hepatic cells than that in the liver of 5-week Western diet WT mice (Figure 2D and Figure S2B). Thus, liver Vsig4+ cells are critical to block the penetration of gut mEVs during the development of NASH.

2.3 | Bacterial DNA accumulation causes fibrogenic activation in HSCs

We observed that depletion of Vsig4+ cells led to increased population of activated HSCs after 5-week Western diet feeding, as evidenced by a greater number of α-SMA+ cells in the Vsig4$^{-/-}$ liver (Figure 2D). In contrast, there were fewer α-SMA+ cells in the liver of 5-week Western diet WT mice (Figure 2D). We also confirmed that HSCs isolated from 5-week Western diet Vsig4$^{-/-}$ mice were at greater degree of fibrogenic activation than WT HSCs, as evidenced by significant greater abundance of fibrosis-associated genes (Figure 3A). Consistently, both Sirius Red and Masson's trichrome staining analyses show that Vsig4$^{-/-}$ mice quickly developed fibrosis in the liver after either 5- or 16-week Western diet feeding, whereas we did not observe significant fibrosis in WT liver (Figure 3B and

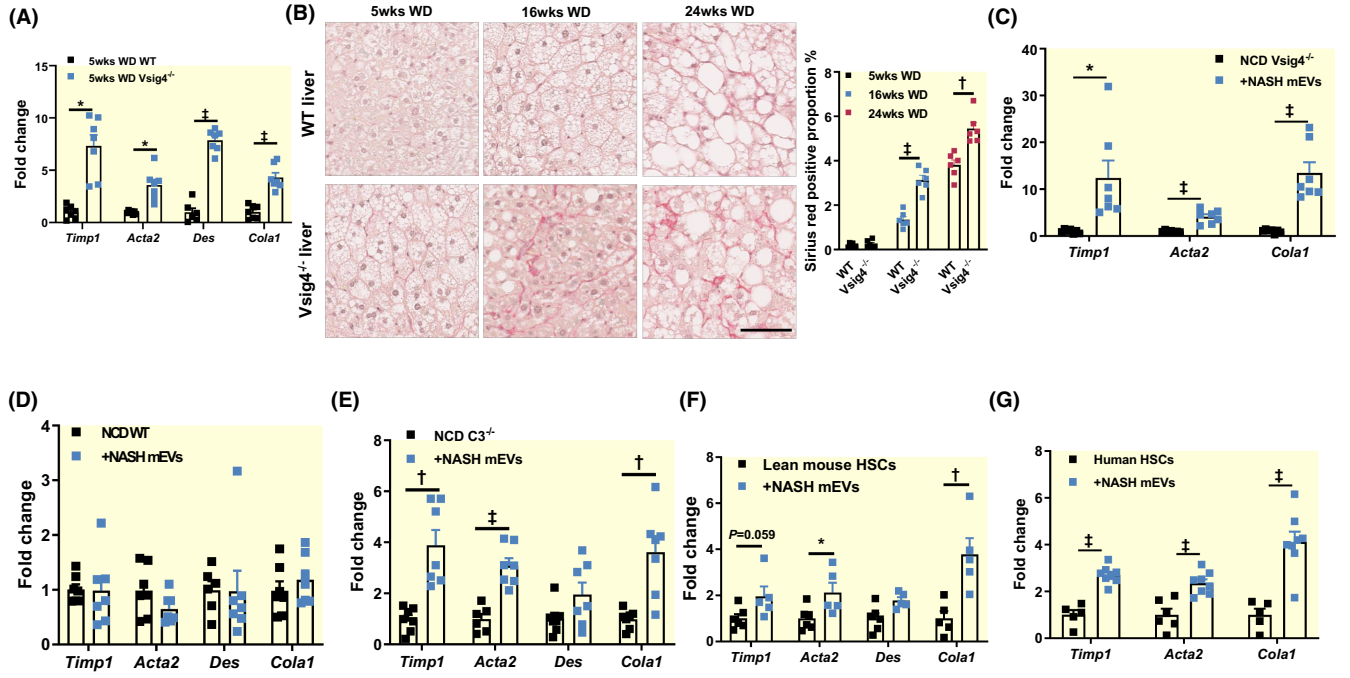

FIGURE 3 NASH mEVs cause fibrogenic activation in HSCs. (A) qPCR analysis of gene abundance associated with fibrogenic activation in 5-week WD-fed WT and Vsig4$^{-/-}$ mice. (B) Sirius Red staining analysis of liver fibrosis in WT and Vsig4$^{-/-}$ mice after feeding WD. Data are the representative of three experiments. Scale bar = 50 μm. Effects of NASH gut mEVs on the expression of fibrogenic genes in the liver of lean Vsig4$^{-/-}$ (C) or WT (D) mice. (E) qPCR analysis of genes associated with fibrogenic activation in the liver of lean C3$^{-/-}$ treated with NASH mEVs. After in vitro treatment with NASH mEVs, qPCR analysis of fibrogenic genes in lean mouse HSCs (F) or human HSCs (G). Data are presented as mean ± SEM. *$p < 0.05$, †$p < 0.01$, ‡$p < 0.001$, Student's t test.

Figure S3A). There was also worsen fibrosis in 24-week Western diet feeding Vsig4$^{-/-}$ liver than NASH WT liver (Figure 3B and Figure S3A).

To mimic the enrichment of gut mEVs in bloodstream in the context of NAFLD/NASH, NASH mEVs were intravenously injected into lean Vsig4$^{-/-}$ mice (1×10^{10} EVs/mouse, twice injection per week) to assess the effects of gut mEVs on the fibrogenic activation in HSCs. While NASH mEV treatment did not affect the body weight (Figure S3B), the key genes associated with fibrogenic activation were elevated in the HSCs isolated from lean Vsig4$^{-/-}$ mice treated with NASH mEVs for 4 weeks (Figure 3C). In contrast, NASH mEV treatment had minimal effect on the fibrogenic activation in the HSCs of lean WT mice (Figure 3D and Figure S3C).

Complement component C3-mediated opsonization plays a crucial role in the ability of Vsig4+ macrophages to interact with bacterial products. While NASH development did not change circulating C3 levels (Figure S3D–F), we observed that NASH mEV treatment results in accumulation of microbial DNAs and elevated fibrogenic activation in HSCs of lean C3$^{-/-}$ mice after 4 weeks treatment with NASH mEVs (Figure 3E).

Given the profound impacts of NASH mEVs on the development of liver fibrosis, we also examined the direct effects of NASH mEVs on in vitro fibrogenic activation in HSCs. Consistent with the improvement induced by NASH mEVs on in vivo HSC fibrogenic activation, lean WT HSCs exhibited elevated abundance of fibrosis-associated genes after exposed to NASH mEVs (1×10^8 EVs per 0.5×10^6 cells; Figure 3F). Healthy human HSCs also enhanced fibrogenic activation after treatment with NASH mEVs (Figure 3G). Overall, these results indicated that penetration of gut mEVs directly leads to fibrogenic activation in HSCs.

2.4 | Bacterial DNA enrichment triggers inflammation in hepatocytes

Inflammatory hepatocytes are key players stimulating fibrogenic activation in HSCs during NASH development. We confirmed that bacterial DNAs were also enriched in the hepatocytes of NASH WT mice (Figure 4A). In addition, in the absence of liver Vsig4+ cells, gut mEVs were infiltrated into hepatocytes, as evidenced by strong red fluorescent signals in the hepatic albumin-expressing cells of NASH WT mice after injection with PKH26-labeled mEVs (Figure 4B). More importantly, after 4 weeks treatment with NASH mEVs, there were greater levels of inflammation in the hepatocytes isolated

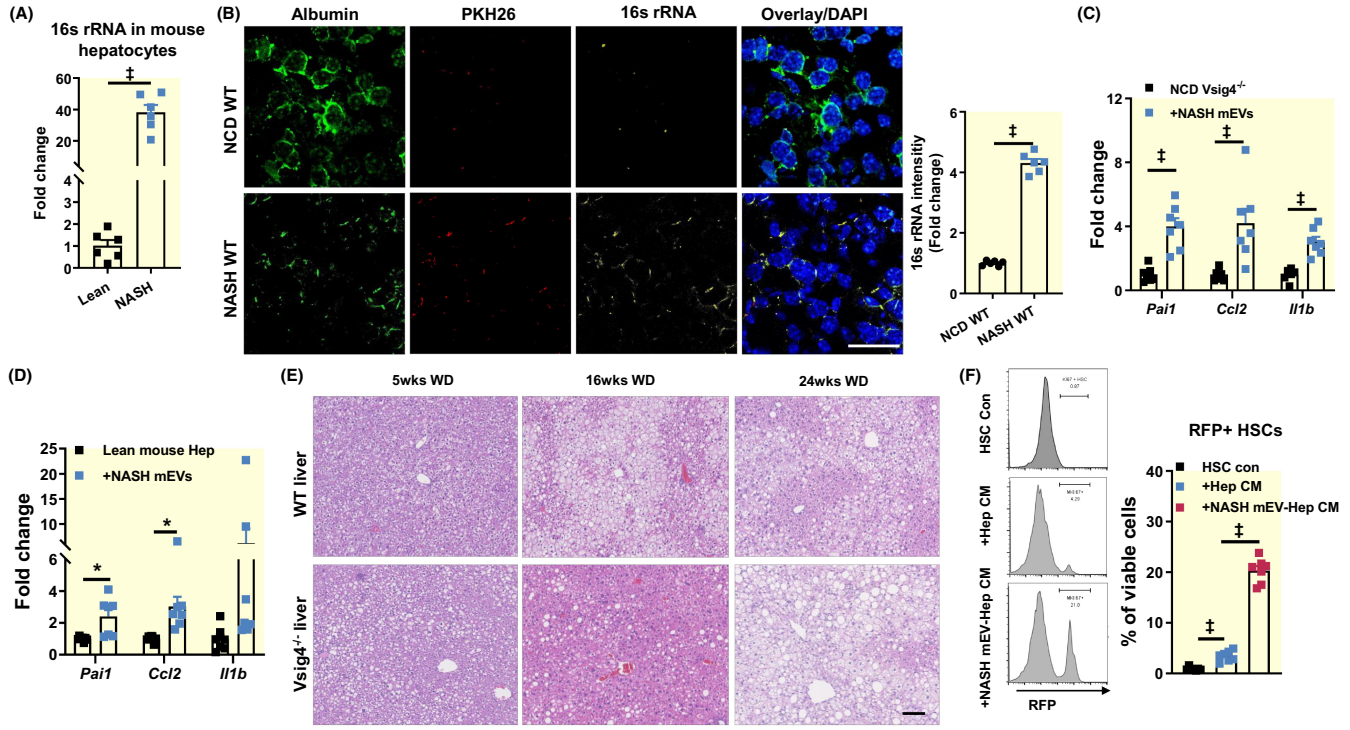

FIGURE 4 NASH mEVs induces hepatocyte inflammation. (A) qPCR analysis of 16s rRNA abundance in mouse hepatocytes. (B) The levels of PKH26 red fluorescence and 16s rRNA in liver albumin+ cells after injection of PKH26-labeled intestinal EVs into the jejunum sections of both NCD and NASH WT mice. (C) After 4-week treatment with NASH mEVs, qPCR analysis proinflammatory mediators in hepatocytes of lean Vsig4$^{-/-}$ mice. The abundance of proinflammatory genes in lean mouse hepatocytes (D) or healthy human hepatocytes (E) after in vitro treatment with NASH mEVs. (F) Flow cytometric analysis of mouse HSC proliferation after co-cultured with conditional mediums derived from NASH mEVs-treated mouse hepatocytes. Data are presented as mean ± SEM. (B,E) Scale bar = 50 μm. *$p < 0.05$, ‡$p < 0.001$, Student's *t* test.

from lean Vsig4$^{-/-}$ or C3$^{-/-}$ mice, as shown by elevated abundance of proinflammatory cytokines or mediators compared to control cells (Figure 4C and Figure S4A). In addition, the degree of inflammatory responses in the hepatocytes of 5-week Western diet Vsig4$^{-/-}$ mice was greater than that in WT mice (Figure S4B). We also confirmed that NASH mEV treatment directly enhanced inflammatory responses in either healthy normal human or lean mouse hepatocytes (Figure 4D and Figure S4C). Additionally, Vsig4$^{-/-}$ mice quickly accumulated lipids in hepatocytes after 5-week Western diet feeding and further developed greater levels of liver steatosis than WT liver after 16- or 24-week Western diet feeding (Figure 4E and Figure S4D).

We also assessed whether NASH mEVs-mediated inflammatory hepatocytes promote proliferation in HSCs. We collected conditional mediums from lean mouse hepatocytes after 24 h treatment with NASH mEVs, and these conditional mediums were used to culture HSCs isolated from lean Mki67 mice (Ki67+ cells express RFP reporter proteins). After 48 h, flow cytometric analysis indicates that adding conditional mediums derived from control hepatocytes without EV treatment (Hep CM) significantly enhanced the proportion of RFP+ proliferating HSCs, compared to control HSCs (Figure 4F). More importantly, treatment with the conditional mediums from NASH mEVs-treated hepatocytes (NASH mEV-Hep CM) led to ~10-fold more RFP+ cells than the effects of Hep CM treatment (Figure 4F). We found that the conditional mediums derived from hepatocytes treated with NASH mEVs contained higher levels of PDGFβ which has been known as a stimulator for HSC proliferation (Figure S4E). Consistently, healthy human hepatocytes secreted greater abundance of PDGFβ after 24 h treatment with NASH mEVs (Figure S4F). In addition, after co-cultured with conditional mediums from NASH mEVs-treated healthy human hepatocytes, the population of Ki67+ human HSCs was also elevated (Figure S4G). We also tested the direct effect of NASH mEVs on HSC proliferation. However, NASH mEV treatment did not directly affect the population of proliferating mouse HSCs (Figure S4H). Therefore, these results suggest that NASH mEVs activates hepatocyte inflammatory responses that can stimulate the proliferation in HSCs.

2.5 | Microbial DNAs are key cargoes for the ability of NASH mEVs

Gut lumen harbors various EVs derived from different types of host cells and microbiota. To demonstrate the critical role of microbiota-derived EVs in the pathogenic effects of NASH gut EVs, we collected gut EVs from Western diet-fed germ-free mice (GF EVs; Figure S5A). After 4-week treatment with GF EVs, both inflammatory responses in hepatocytes and fibrogenic activation in HSCs of lean Vsig4$^{-/-}$ mice were comparable with control recipients (Figure 5A,B). We further assessed the importance of microbial DNA cargoes within gut EVs. Microbial DNAs were depleted from NASH gut EVs (DNA-free EVs) using our previously reported method (Figure S5A).[43] We observed that these DNA-free EVs did not change the responses of hepatic cells in lean Vsig4$^{-/-}$ mice (Figure 5A,B). Consistent with these in vivo phenotypes, GF EVs or DNA-free EVs did not affect the responses of mouse or human hepatocytes or HSCs in in vitro experiments (Figure 5C,D and Figures S4C and S5B). In contrast, microbial DNA-containing gut EVs collected from NASH WT mice (NASH mEV) significantly enhanced hepatic inflammation and fibrogenic activation in both in vivo and in vitro experiments (Figure 5A–D and Figures S4C and S5B). Thus, these data demonstrate that microbial DNAs are key cargoes contributing to the pathogenic effects of NASH gut EVs.

2.6 | cGAS/STING signaling is critical for the ability of microbial DNA to induce hepatic dysfunction

Previous studies, including ours, have demonstrated that the activation of cGAS/STING pathway is important for bacterial DNA-induced cellular responses. We observed that bacterial DNA accumulation was accompanied by greater levels of cGAS and phosphorylated STING in the HSCs isolated from 5-week Western diet Vsig4$^{-/-}$ mice

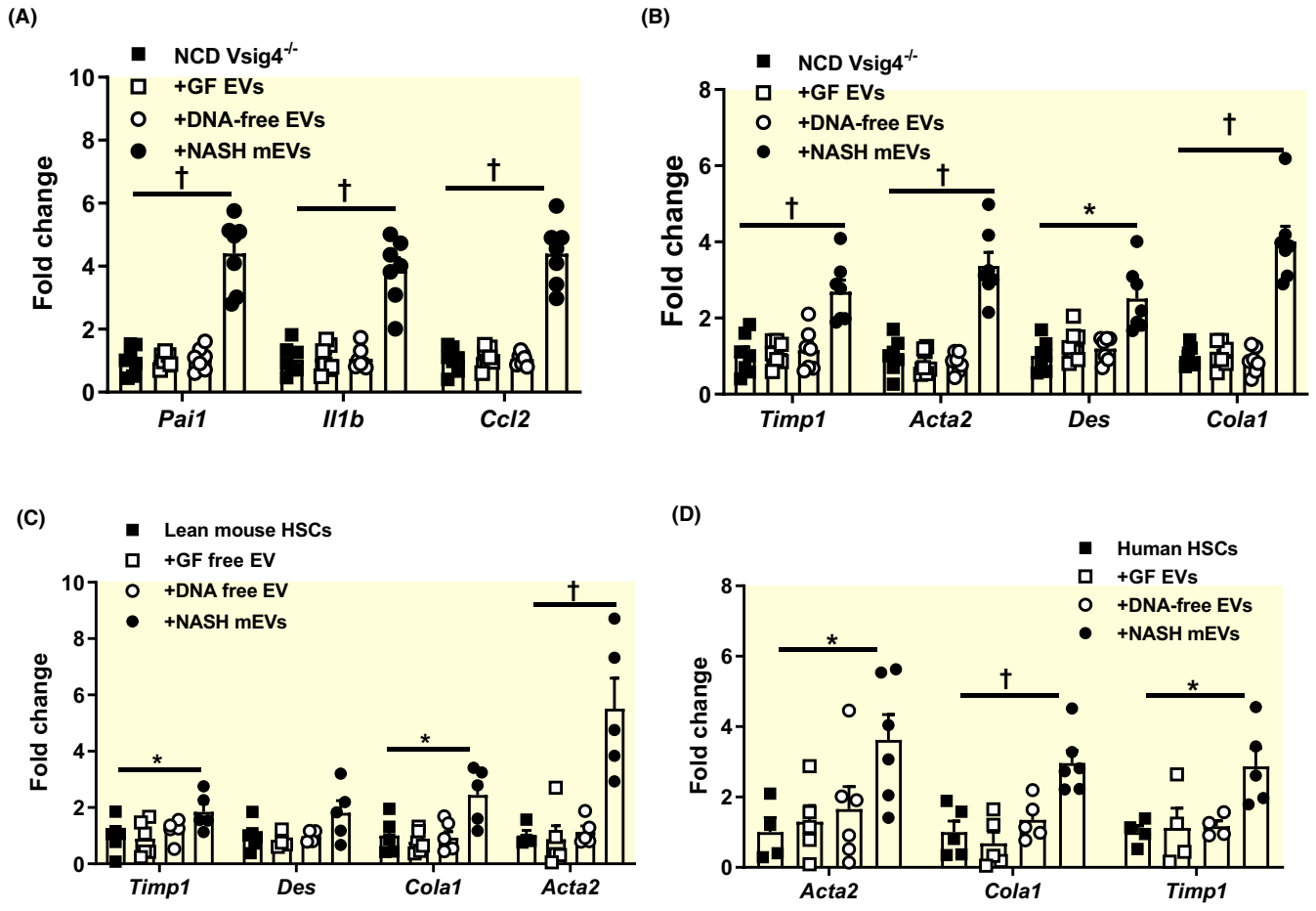

FIGURE 5 Microbial DNAs are pathogenic cargoes for the effects of NASH mEVs. qPCR analysis of the expression of proinflammatory genes in hepatocytes (A) and fibrogenic genes (B) in the HSCs of lean Vsig4$^{-/-}$ recipient mice treated with either NASH mEVs, NASH germ-free (GF) EVs, or NASH DNA-free EVs. Effects of intestinal EVs on the abundance of fibrogenic genes in mouse (C) or human (D) HSCs. Data are presented as mean ± SEM. *$p < 0.05$, †$p < 0.01$, Student's t test.

or NASH mEV-treated lean Vsig4$^{-/-}$ mice (Figure 6A,B). In addition, in vitro treatment with NASH mEVs led to increased activation of cGAS/STING signaling in either mouse or human hepatic cells (Figure 6C,D and Figure S6A,B).

To further assess the importance of cGAS/STING pathway on the ability of microbial DNAs to induce hepatic dysfunction, 5-week Western diet cGAS$^{-/-}$ mice were intravenously injected with NASH mEVs (1×10^{10} EVs/mouse, twice injection per week). After 4-week treatment, there were comparable levels of hepatocyte inflammation and HSC fibrogenic activation among these cGAS$^{-/-}$ mice, as shown by no difference in the abundance of proinflammatory mediators and fibrosis-associated genes (Figure 6E,F and Figure S6C). In the in vitro experiments using hepatocytes or HSCs isolated from lean cGAS$^{-/-}$ mice, we also observed that NASH mEVs did not significantly affect cellular responses (Figure 6G,H). Similarly, knockdown of cGAS in healthy human hepatocytes or HSCs blunted the effects of NASH mEVs (Figure 6I,J). In addition, we observed less steatosis in Western diet-fed cGAS$^{-/-}$ mice, compared to that in NASH WT liver (Figure S6D,E). Knockout of cGAS also blunted the formation of fibrosis in liver, as shown by barely detectable Sirius Red or Masson's trichrome staining signals in 24-week Western diet cGAS$^{-/-}$ liver (Figure 6K and Figure S6F). Taking together, these results demonstrate the critical role of cGAS/STING signaling for the effects of microbial DNAs on host hepatic cells.

3 | DISCUSSION

In this study, we have evaluated the effects of microbial DNA accumulation on the activation of hepatic inflammation and fibrogenic activation that contribute to NASH development. In specific, we find that intestinal mEVs can pass through impaired gut barrier and deliver microbial DNAs into hepatic cells, subsequently causing cellular inflammation and fibrogenic activation in liver. Hepatic Vsig4+ cells play a critical role in protecting hepatocytes and HSCs from the infiltration of gut mEVs through a C3-dependent mechanism, whereas knockout of Vsig4 or C3

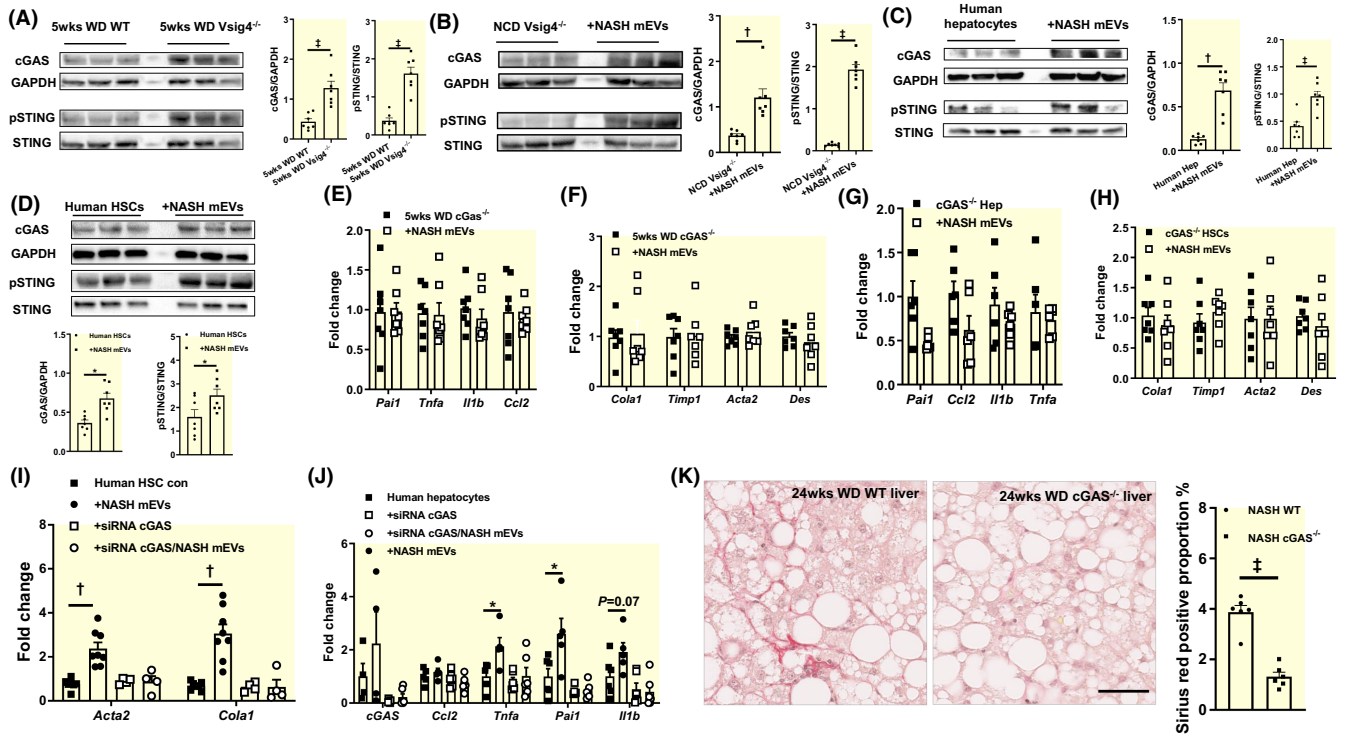

FIGURE 6 The activation of cGAS/STING pathway plays a critical role in microbial DNA-induced liver dysfunctions. (A) The levels of cGAS and STING phosphorylation in the liver of WT and Vsig4$^{-/-}$ mice after 5-week WD feeding. (B) Effects of NASH mEVs on the activation of cGAS/STING pathway in HSCs of lean Vsig4$^{-/-}$ mice after 4-week treatment with NASH mEVs. The levels of cGAS/STING activation in healthy human hepatocytes (C) or HSCs (D) after in vitro treatment with NASH mEVs. The influence of cGAS ablation on the responses of hepatocytes (E) and HSCs (F) to NASH mEV treatment. The proinflammatory genes in lean cGAS$^{-/-}$ hepatocytes (G) and fibrogenic genes in lean cGAS$^{-/-}$ HSCs (H) after in vitro treatment with NASH mEVs. Effects of NASH mEVs on the responses of human HSCs (I) and hepatocytes (J) with cGAS knockdown. (K) Liver fibrosis evaluated by Sirius red staining analysis. Scale bar = 50 μm Data are presented as mean ± SEM. *$p < 0.05$, †$p < 0.01$, Student's t test.

blunt the ability of liver macrophages to block the pathogenesis of gut mEVs. We observe minimal effects of gut EVs collected from germ-free mice on liver dysfunction, thus indicating the critical role microbiota-derived EVs in the gut EVs. Furthermore, the microbial DNA cargoes are responsible for these effects of NASH gut EVs, as evidenced by diminished effects of gut EVs after depletion of microbial DNAs. Finally, we confirm that the activation of cGAS/STING signaling is important for microbial DNAs to trigger inflammation and fibrogenic activation in hepatic cells in both in vivo and in vitro experiments.

An impaired gut barrier is a feature of obesity.[21–25] Previous study has demonstrated that overweight is accompanied by microbial DNA accumulation in key metabolic tissues.[36,43,45] As expected, we also find that bacterial DNA enrichment is occurred in both hepatocytes and HSCs in NASH mouse and human liver. Several studies also report that bacterial DNA abundance is elevated in the circulation and liver of NAFLD/NASH humans or mice. More importantly, we further validate that gut mEVs play a critical role in transferring microbial DNAs into hepatic cells in the context of gut barrier breach.

Previous studies have demonstrated that liver Vsig4+ macrophages are key players exerting protection for other hepatic cells from the pathogenesis of bacterial products.[42,43] In line with our previous findings, in the absence of liver Vsig4+ cells, gut mEVs efficiently infiltrate into both hepatocytes and HSCs in lean Vsig4$^{-/-}$ mice. In contrast, there is barely detectable bacterial DNA in the Vsig4+ cell-enriched liver of lean WT mice. In both NASH human and mouse liver, Vsig4 abundance was markedly reduced, subsequently elevating the susceptibility of host cells to the impacts of bacterial products. We have observed that bacterial DNA accumulation in bloodstream quickly occurred after 5-week WD feeding, whereas no significant increase in bacterial DNA detected in the liver of 5-week WD WT mice. In addition, liver Vsig4+ macrophage population was not significantly changed after 5-week WD feeding but diminished after 24-week WD feeding, thus suggesting that loss of Vsig4 likely causes bacterial DNA enrichment in host cells in NASH livers. In addition to the Vsig4-dependent function, previous studies have shown that macrophages can exert phagocytosis on bacterial products through other mechanisms, such as scavenger receptors.[46] It has been known that C3-mediated opsonization is important for the ability of Vsig4+ macrophages to interact with bacterial products. Indeed, we found that knockout of C3 blunted the interaction between Vsig4+ macrophages and gut mEVs. Previously, Zeng et al suggest that bacterial lipoteichoic acid (LTA) component can be recognized by liver Vsig4+ macrophages.[47] However, we found that there was undetectable level of LTA within NASH mEVs (data not shown), thus suggesting the minimal effect of LTA on the ability of Vsig4+ macrophages to bind gut mEVs. In addition to the ability to clean bacterial products from bloodstream, liver Visg4+ macrophages may regulate hepatic inflammation status through other mechanisms such as the secretion of cytokines or exosomes.

Emerging evidence indicates the pathogenic roles of various microbiota-derived products in fueling the development of metabolic diseases.[26] Our findings support that translocation of microbiota-secreted EVs into liver can cause hepatic inflammation and fibrogenic activation, as evidenced by elevated hepatocyte inflammation and HSC activation in either lean Vsig4$^{-/-}$ or C3$^{-/-}$ mice after injection with NASH mEVs. While various types of host cells also secrete EVs into gut lumen, the EVs from germ-free mice had minimal effects on hepatic cell functions. Thus, this suggests that microbiota-derived EVs are pathogenic within gut EVs. However, a previous study reports that intestinal epithelial cell-derived EVs can blunt the development of inflammatory bowel disease by regulating intestinal tract immune balance.[48]

In line with previous findings that enrichment of bacterial DNAs leads to host cell dysfunction, our data support that microbial DNA is a pathogenic mediator triggering NAFLD/NASH-associated hepatic inflammation and fibrogenic activation. In line with inflammation as an inducer for NAFLD phenotypes, we observed that Vsig4$^{-/-}$ mice quickly accumulated lipids in liver after Western diet feeding. In addition, microbial DNA-induced hepatocyte inflammation elevated the secretion of PDGFβ for HSC proliferation. More importantly, the microbial DNA cargo is the key molecule for the pathogenic effects of gut EVs, as evidenced by minimal effects of DNA-free gut EVs on hepatic cell responses. However, previous studies suggest that gut microbiota-derived outer membrane vesicles carry polysaccharide or a variety of digesting enzymes that modulate intestinal immune cell responses.[49,50] It has been known that there are marked differences in cargo components among various types of EVs, thus leading to the distinct observations from ours and previous findings from the outer membrane vesicles.

Previous studies, including ours, have demonstrated that activation of cGAS/STING pathway is critical for microbial DNAs to initiate host cell dysfunction.[43,51] Indeed, we observed microbial DNA accumulation was concomitant with elevated abundance of cGAS and phosphorylated STING in hepatic cells. Luo et al[52] have shown that STING depletion can ameliorate liver inflammation and fibrogenic activation. Our previous study also observes that cGAS knockout blunts the effects of microbial DNAs on the inflammatory responses of insulin-sensitizing cells.[43] Consistently, in our study, hepatic cells without cGAS displayed minimal responses to microbial

DNA accumulation. Therefore, these demonstrate the importance of cGAS/STING signaling on the microbial DNA-induced hepatic cell responses. In addition to cGAS/STING pathway, the nucleotide-binding oligomerization domain (NOD) proteins can sense bacterial infection through binding to bacterial peptidoglycans, g-D-glutamyl-meso-diaminopimelic acid, and/or muramyl dipeptide, triggering cellular inflammatory responses.[53] However, it is still unknown that microbiota-derived EVs harbor NOD ligands that can induce the activation of NOD-related pathways. In addition, it is possible that microbial DNA enrichment-induced host cell death led to the release of DNA fragments which could trigger cGAS/STING activation.

In summary, we have shown that during the course of NAFLD/NASH, microbial DNAs exert profound effects to fuel inflammation and fibrogenic activation in liver through a cGAS/STING-dependent mechanism. These studies hold significant potential for therapeutic intervention. One can envision that restoring Vsig4+ macrophages could block the infiltration of gut mEVs and accumulation of microbial DNAs in hepatic cells. In addition, it is possible that cGAS/STING could be therapeutic targets against microbial DNA-induced cellular abnormalities.

4 | MATERIALS AND METHODS

4.1 | Mouse information

Wild-type (WT) C57BL6, $C3^{-/-}$, $cGAS^{-/-}$, and Mki67 mice were received from the Jackson Laboratory. $Vsig4^{-/-}$ mice (C57BL/6 background) were maintained by Dr Wei Ying laboratory. The Vsig4 wild-type (WT) mice were produced by crossing $Vsig4^{\pm}$ heterozygous mice together. Germ-free (GF) C57BL/6 mice were maintained in the UCSD Gnotobiotic Mouse Facility. All mice were maintained on a 12/12-h light–dark cycle. At 12 weeks of age, male mice were used as recipients for gut extracellular vesicle (EV) injection. Mice were fed a Western diet (AIN76A; 20% milk fat, 0.2% cholesterol, and 34% sucrose by weight; TestDiet® 5342) or a normal chow diet (5.1% mixture of milk fat/lard/soybean oil/corn oil, 10% sucrose by weight; TestDiet® 5TJS).

4.2 | Institutional review board statement

All animal procedures were done in accordance with the University of California, San Diego Research Guidelines for the Care and Use of Laboratory Animals. The UCSD IRB has waived the review and approval for the usage of human liver samples (UCSD IRB exempt protocol #801545) due to the secondary usage of existing human liver biospecimens.

4.3 | Gut EV isolation and characterization

Feces were collected from small intestine sections of NASH WT mice in sterile PBS buffer in a sterile hood. To remove debris and dead cells, the samples were spined at 1000 ***g*** for 10 min, 4°C. The samples were passed through 0.22 μm filters and then ultracentrifugated at 100 000 ***g*** for 4 h at 4°C. The EV-containing pellets were resuspended in sterile PBS buffer and passed through 0.22 μm filters. EV concentration and particle size were evaluated by the NanoSight analysis (Malvern Instruments). Each EV sample was measured at least three times using the Nanoparticle Tracking Analysis software with default settings (camera level = 10–11, temperature = 25–26°C).

4.4 | In vivo EV trafficking assays

PKH26-labeled EVs (1×10^{10} EVs per mouse in 200 μl of sterile PBS) were introduced to either lean or NASH recipient mice through either injection into jejunum section or tail vein. Livers were collected for measuring the intensity of PKH26 red fluorescence.

4.5 | In vivo and in vitro gut mEV treatment

For in vitro treatment, 1×10^5 hepatic stellate cells and hepatocytes were treated with 1×10^8 EVs for 24–36 h, then used for relevant test. For in vivo treatment, recipient mice were treated with 1×10^{10} EVs twice per week through tail vein injection.

4.6 | Hepatocyte isolation

Briefly, mice were infused with a calcium-free HEPES-phosphate buffer A (calcium- and magnesium-free PBS containing 10 mM HEPES, 0.2 uM EGTA, 0.2% BSA, and 1 mM glucose, pH 7.4) via the vena cava. After liver appeared to a light brown or beige color, collagenase-containing buffer B (PBS with 1 mM calcium, 0.2% BSA, 1 mM magnesium, and 30 mM HEPES, 0.5 mg collagenase D/ml) was perfused until cracking signs on the liver surface. Then, the liver was harvested, and cells were released from digested livers in ice-cold Buffer A.

After filtered through a 100-μm nylon filter, cells were centrifuged at 50 ***g*** for 5 min at 4°C. After washed with Buffer A twice, cells were mixed with Percoll (using 10× PBS to adjust to the physiological ionic strength, the final concentration = 36%) and then centrifuged at 100 ***g*** for 10 min, 4°C. After removing the supernatant, the hepatocyte pellet was resuspended with Buffer A and spined at 50 ***g*** for 5 min at 4°C. Finally, hepatocytes were cultured with Williams Medium E containing 10% FBS and 10 nM dexamethasone on collagen-coated plates and antibiotics. Cryopreserved and plateable healthy human hepatocytes were received from Lonza.

4.7 | HSC isolation

Mouse liver was sequentially perfused via superior vena cava first with 30–40 ml of calcium-free HEPES-phosphate buffer A, next with 30 ml of 0.5 mg/ml pronase, and finally with 30 ml of 0.5 mg/ml collagenase D. After digestion of the clipped liver tissue in a mixture containing pronase, DNase I, and collagenase D for 20 min, the cell suspension was centrifuged at 50 ***g*** for 3 min to further remove liver parenchymal cells. The supernatant was collected, and then, non-parenchymal cells were harvested after centrifuging at 900 ***g*** for 8 min at 4°C. The non-parenchymal cell pellet was resuspended in 15% OptiPrep buffer and transferred to a 15-ml centrifuge tube. Then, 5 ml of 11.5% OptiPrep and 2 ml of Gey's Balanced Salt Solution (GBSS; Sigma-Aldrich) were sequentially layered onto the cell suspension. After spined at 2000 g for 20 min at 4°C with low acceleration, HSCs between the 11.5% OptiPrep and GBSS were carefully collected. These cells were washed twice (800 g for 10 min, 4°C) and then seeded with culture medium (1% Glutax, 10% FBS, and 2% penicillin/streptomycin) at 37°C. Cryopreserved human stellate cells (passage 1) were received from Lonza.

4.8 | siRNA transfection

siRNA-cGAS (Cat. No. J-015607-17-0002; Horizon Discovery) was mixed with RNAiMAX reagent. This mixture was co-cultured with human HSCs or hepatocytes (20 pmol siRNA for 0.1×10^6 cells) for 24 h.

4.9 | Quantification of bacterial DNA using real-time PCR

A Femto Bacterial DNA Quantification Kit was used to measure bacterial DNA abundance, according to the manufacturer's instructions (Cat. No. D4301, Zymo Research).

4.10 | Immunofluorescent staining

Immunostaining was performed as previously described. Briefly, mouse liver frozen sections (4–6 mm thickness) were fixed with cold acetone for 20 min. After treated with 5% normal donkey serum for 60 min at RT, antibodies (diluted 1:100–1:500 in PBS) were added to the samples for overnight incubation at 4°C. DAPI was used to stain nucleus for 10 min at RT. The Leica SP8 Confocal microscope was used to take images.

4.11 | Liver histology analysis

Liver sections were analyzed by H&E, Sirius Red, or Masson's trichrome staining at UCSD Moore Cancer center histology core. The NanoZoomer slide scanner was used to scan images. The Sirius red positive areas were measured by imageJ. Steatosis in more than 5% of hepatocytes is necessary for a diagnosis of NAFLD.

4.12 | RNAscope in situ hybridization (ISH) combined with immunofluorescence

RNAscope ISH assays were used to detect 16s RNA. Liver cryosections (10 μm thickness) were fixed with 4% PFA for 15 min at 4℃, After dehydrated with 50%, 70%, and 100% ethyl alcohol gradients sequentially (5 min for each step, RT), the sections were treated by hydrogen peroxide (ACDBio; 10 min) and then protease IV (ACDBio; 10 min) at RT. Then, slides were incubated with 16s RNA probes (ACDBio) for 2 h at 40°C. The slides were then incubated with signal amplification and detection reagents (AMP 1, AMP 2, AMP 3, HRP-C1, Opal 520; ACDBio). Finally, the slides were immediately processed for immunofluorescence, and images were taken using the Leica SP8 Confocal microscope. Human liver sections (5 μm thickness) were obtained from the University of Minnesota Liver Tissue and Cell Distribution Service (UM-LTCDS).

4.13 | HSC proliferation assay

HSC proliferation assay is performed by flow cytometry. Briefly, after the HSCs were obtained from lean Mki67 mice as described above, the cells were cultured with the conditional medium derived from lean mouse hepatocytes treated with NASH gut mEVs or empty liposomes. After 48 h, the population of RFP+ (Ki67+) HSCs was measured by flow cytometric analysis. Similarly, lean healthy human HSCs were cultured with the conditional medium derived from healthy human hepatocytes treated

with NASH mEVs or empty liposomes. After 48 h, human HSCs were intracellularly stained with anti-Ki67 antibody, and Ki67+ HSC population was measured by flow cytometric analysis. HSCs without hepatocyte-derived conditional medium were used as controls.

4.14 | Quantitative reverse transcriptase-polymerase chain reaction (RT-PCR) analysis

The Quick-RNA Microprep kits (Zymo Research) were used to purified total RNAs from tissues or cells. RNA concentration was measured using a NanoDrop spectrophotometer. SuperScript III and random hexamers were used for reverse transcription reactions. iTaq SYBR Green supermix was used for quantitative PCR on a StepOnePlus Real-Time PCR Systems (ThermoFisher Scientific).

4.15 | Western blot analysis

Proteins were extracted from tissues or cells with RIPA lysis buffer and then concentration was determined by DC™ protein assays (BIO-RAD Laboratories). After processed with 4x Laemmli protein sample buffer (BIO-RAD Laboratories), the protein samples were loaded onto Mini-PROTEAN TGX precast gels (BIO-RAD Laboratories). After gel electrophoresis, proteins were then transferred to a PVDF membrane and blocked using 5% non-fat milk for at least 30 min. Primary antibodies were incubated with membranes overnight at 4°C. After incubated with secondary antibody at room temperature for 45 min, the signal intensity was measured with chemiluminescent substrates on a ChemiDoc imaging system (BIO-RAD Laboratories).

4.16 | Statistical analysis

The results were obtained from ≥2 independent experiments, and the data are expressed as the mean ± SD. p values of 0.05 or less indicate statistical differences. Statistical analyses were measured with unpaired two-tailed Student's t test using Prism8 software.

ACKNOWLEDGMENTS

We thank Jennifer Santini for confocal microscope; UCSD histology core for H&E, Sirius Red, and Masson's trichrome staining analysis; Dr Mojgan Hosseini for liver steatosis and fibrosis evaluation. This study was funded by the UCSD School of Medicine Microscopy Core grant (P30 NS047101), the National Natural Science Foundation of China (no. 81500436 to Z. L.), and the US National Institute of Diabetes and Digestive and Kidney Diseases R00 award (R00DK115998 to W. Y.), R01 award (R01DK125560 to W. Y.), and the UCSD/UCLA Diabetes Research Center Pilot and Feasibility grant (P30 DK063491 to W. Y.).

CONFLICT OF INTEREST

The authors declare no conflict of interest.

AUTHOR CONTRIBUTIONS

WY conceived the project and designed experiments; ZL and YJ performed most of the experiments; DZ, HG, ZJ, and MY assisted with immunofluorescent analysis, tissue collection, cell culture, qPCR analysis, and flow cytometric analysis; DZ performed experiments for revision. WY supervised the project; YJ, ZL, and WY analyzed and interpreted the data and co-wrote the manuscript.

DATA AVAILABILITY STATEMENT

The datasets generated in the current study are available from the corresponding authors upon reasonable request. There are no restrictions on data availability.

ORCID

Wei Ying https://orcid.org/0000-0002-4890-7256

REFERENCES

1. Younossi Z, Tacke F, Arrese M, et al. Global perspectives on nonalcoholic fatty liver disease and nonalcoholic steatohepatitis. *Hepatology*. 2019;69(6):2672-2682.
2. Loomba R, Sanyal AJ. The global NAFLD epidemic. *Nat Rev Gastroenterol Hepatol*. 2013;10(11):686-690.
3. Younossi ZM, Koenig AB, Abdelatif D, Fazel Y, Henry L, Wymer M. Global epidemiology of nonalcoholic fatty liver disease-meta-analytic assessment of prevalence, incidence, and outcomes. *Hepatology*. 2016;64(1):73-84.
4. Koyama Y, Brenner DA. Liver inflammation and fibrosis. *J Clin Invest*. 2017;127(1):55-64.
5. Schuster S, Cabrera D, Arrese M, Feldstein AE. Triggering and resolution of inflammation in NASH. *Nat Rev Gastroenterol Hepatol*. 2018;15(6):349-364.
6. Mridha AR, Wree A, Robertson AAB, et al. NLRP3 inflammasome blockade reduces liver inflammation and fibrosis in experimental NASH in mice. *J Hepatol*. 2017;66(5):1037-1046.
7. Kakisaka K, Cazanave SC, Fingas CD, et al. Mechanisms of lysophosphatidylcholine-induced hepatocyte lipoapoptosis. *Am J Physiol Gastrointest Liver Physiol*. 2012;302(1):G77-84.
8. Kawano Y, Cohen DE. Mechanisms of hepatic triglyceride accumulation in non-alcoholic fatty liver disease. *J Gastroenterol*. 2013;48(4):434-441.
9. Min H-K, Kapoor A, Fuchs M, et al. Increased hepatic synthesis and dysregulation of cholesterol metabolism is associated with the severity of nonalcoholic fatty liver disease. *Cell Metab*. 2012;15(5):665-674.
10. Feldstein AE, Werneburg NW, Canbay A, et al. Free fatty acids promote hepatic lipotoxicity by stimulating

TNF-alpha expression via a lysosomal pathway. *Hepatology*. 2004;40(1):185-194.
11. Takahashi S, Luo Y, Ranjit S, et al. Bile acid sequestration reverses liver injury and prevents progression of nonalcoholic steatohepatitis in Western diet-fed mice. *J Biol Chem*. 2020;295(14):4733-4747.
12. Ferslew BC, Xie G, Johnston CK, et al. Altered bile acid metabolome in patients with nonalcoholic steatohepatitis. *Dig Dis Sci*. 2015;60(11):3318-3328.
13. Arab JP, Karpen SJ, Dawson PA, Arrese M, Trauner M. Bile acids and nonalcoholic fatty liver disease: molecular insights and therapeutic perspectives. *Hepatology*. 2017;65(1):350-362.
14. Karlmark KR, Weiskirchen R, Zimmermann HW, et al. Hepatic recruitment of the inflammatory Gr1+ monocyte subset upon liver injury promotes hepatic fibrosis. *Hepatology*. 2009;50(1):261-274.
15. Zimmermann HW, Seidler S, Nattermann J, et al. Functional contribution of elevated circulating and hepatic non-classical CD14CD16 monocytes to inflammation and human liver fibrosis. *PLoS One*. 2010;5(6):e11049.
16. Seki E, de Minicis S, Inokuchi S, et al. CCR2 promotes hepatic fibrosis in mice. *Hepatology*. 2009;50(1):185-197.
17. Luedde T, Kaplowitz N, Schwabe RF. Cell death and cell death responses in liver disease: mechanisms and clinical relevance. *Gastroenterology*. 2014;147(4):765-783 e764.
18. Hirsova P, Gores GJ. Death receptor-mediated cell death and proinflammatory signaling in nonalcoholic steatohepatitis. *Cell Mol Gastroenterol Hepatol*. 2015;1(1):17-27.
19. Feldstein AE, Canbay A, Angulo P, et al. Hepatocyte apoptosis and fas expression are prominent features of human nonalcoholic steatohepatitis. *Gastroenterology*. 2003;125(2):437-443.
20. Wang P-X, Ji Y-X, Zhang X-J, et al. Targeting CASP8 and FADD-like apoptosis regulator ameliorates nonalcoholic steatohepatitis in mice and nonhuman primates. *Nat Med*. 2017;23(4):439-449.
21. Levy M, Kolodziejczyk AA, Thaiss CA, Elinav E. Dysbiosis and the immune system. *Nat Rev Immunol*. 2017;17(4):219-232.
22. Cani PD, Amar J, Iglesias MA, et al. Metabolic endotoxemia initiates obesity and insulin resistance. *Diabetes*. 2007;56(7):1761-1772.
23. Jin X, Yu CH, Lv GC, Li YM. Increased intestinal permeability in pathogenesis and progress of nonalcoholic steatohepatitis in rats. *World J Gastroenterol*. 2007;13(11):1732-1736.
24. Johnson AMF, Costanzo A, Gareau MG, et al. High fat diet causes depletion of intestinal eosinophils associated with intestinal permeability. *PLoS One*. 2015;10(4):e0122195.
25. Thaiss CA, Levy M, Grosheva I, et al. Hyperglycemia drives intestinal barrier dysfunction and risk for enteric infection. *Science*. 2018;359(6382):1376-1383.
26. Tilg H, Zmora N, Adolph TE, Elinav E. The intestinal microbiota fuelling metabolic inflammation. *Nat Rev Immunol*. 2020;20(1):40-54.
27. Wollam J, Riopel M, Xu YJ, et al. Microbiota-produced N-formyl peptide fMLF promotes obesity-induced glucose intolerance. *Diabetes*. 2019;68(7):1415-1426.
28. Zhao L, Zhang F, Ding X, et al. Gut bacteria selectively promoted by dietary fibers alleviate type 2 diabetes. *Science*. 2018;359(6380):1151-1156.
29. Koh A, Molinaro A, Ståhlman M, et al. Microbially produced imidazole propionate impairs insulin signaling through mTORC1. *Cell*. 2018;175(4):947-961 e917.
30. Rothhammer V, Borucki DM, Tjon EC, et al. Microglial control of astrocytes in response to microbial metabolites. *Nature*. 2018;557(7707):724-728.
31. Tang WHW, Wang Z, Levison BS, et al. Intestinal microbial metabolism of phosphatidylcholine and cardiovascular risk. *N Engl J Med*. 2013;368(17):1575-1584.
32. Wang Z, Klipfell E, Bennett BJ, et al. Gut flora metabolism of phosphatidylcholine promotes cardiovascular disease. *Nature*. 2011;472(7341):57-63.
33. Puri P, Liangpunsakul S, Christensen JE, et al. The circulating microbiome signature and inferred functional metagenomics in alcoholic hepatitis. *Hepatology*. 2018;67(4):1284-1302.
34. Lelouvier B, Servant F, Païssé S, et al. Changes in blood microbiota profiles associated with liver fibrosis in obese patients: a pilot analysis. *Hepatology*. 2016;64(6):2015-2027.
35. Amar J, Chabo C, Waget A, et al. Intestinal mucosal adherence and translocation of commensal bacteria at the early onset of type 2 diabetes: molecular mechanisms and probiotic treatment. *EMBO Mol Med*. 2011;3(9):559-572.
36. Anhê FF, Jensen BAH, Varin TV, et al. Type 2 diabetes influences bacterial tissue compartmentalisation in human obesity. *Nat Metab*. 2020;2:233-242.
37. Ortiz S, Zapater P, Estrada JL, et al. Bacterial DNA translocation holds increased insulin resistance and systemic inflammatory levels in morbid obese patients. *J Clin Endocrinol Metab*. 2014;99(7):2575-2583.
38. Kimura I, Miyamoto J, Ohue-Kitano R, et al. Maternal gut microbiota in pregnancy influences offspring metabolic phenotype in mice. *Science*. 2020;367(6481):eaaw8429. 10.1126/science.aaw8429
39. Mathieu M, Martin-Jaular L, Lavieu G, Thery C. Specificities of secretion and uptake of exosomes and other extracellular vesicles for cell-to-cell communication. *Nat Cell Biol*. 2019;21(1):9-17.
40. Liu Y, Defourny KAY, Smid EJ, Abee T. Gram-positive bacterial extracellular vesicles and their impact on health and disease. *Front Microbiol*. 2018;9:1502.
41. Chelakkot C, Choi Y, Kim D-K, et al. Akkermansia muciniphila-derived extracellular vesicles influence gut permeability through the regulation of tight junctions. *Exp Mol Med*. 2018;50(2):e450.
42. Helmy KY, Katschke KJ, Gorgani NN, et al. CRIg: a macrophage complement receptor required for phagocytosis of circulating pathogens. *Cell*. 2006;124(5):915-927.
43. Luo Z, Ji Y, Gao H, et al. CRIg(+) macrophages prevent gut microbial DNA-containing extracellular vesicle-induced tissue inflammation and insulin resistance. *Gastroenterology*. 2021;160(3):863-874.
44. Mouries J, Brescia P, Silvestri A, et al. Microbiota-driven gut vascular barrier disruption is a prerequisite for non-alcoholic steatohepatitis development. *J Hepatol*. 2019;71(6):1216-1228.
45. Oh TG, Kim SM, Caussy C, et al. A universal gut-microbiome-derived signature predicts cirrhosis. *Cell Metab*. 2020;32(5):878-888 e876.
46. Broadley S, Plaumann A, Coletti R, et al. Dual-track clearance of circulating bacteria balances rapid restoration of blood sterility with induction of adaptive immunity. *Cell Host Microbe*. 2016;20(1):36-48.
47. Zeng Z, Surewaard BG, Wong CH, Geoghegan JA, Jenne CN, Kubes P. CRIg functions as a macrophage pattern recognition

receptor to directly bind and capture blood-borne gram-positive bacteria. *Cell Host Microbe*. 2016;20(1):99-106.
48. Jiang L, Shen Y, Guo D, et al. EpCAM-dependent extracellular vesicles from intestinal epithelial cells maintain intestinal tract immune balance. *Nat Commun*. 2016;7:13045.
49. Fabrega MJ, Aguilera L, Gimenez R, et al. Activation of immune and defense responses in the intestinal mucosa by outer membrane vesicles of commensal and probiotic escherichia coli strains. *Front Microbiol*. 2016;7:705.
50. Ahmadi Badi S, Moshiri A, Fateh A, et al. Microbiota-derived extracellular vesicles as new systemic regulators. *Front Microbiol*. 2017;8:1610.
51. Ablasser A, Chen ZJ. cGAS in action: expanding roles in immunity and inflammation. *Science*. 2019;363(6431):eaat8657.
52. Luo X, Li H, Ma L, et al. Expression of STING is increased in liver tissues from patients with NAFLD and promotes macrophage-mediated hepatic inflammation and fibrosis in mice. *Gastroenterology*. 2018;155(6):1971-1984 e1974.
53. Caruso R, Warner N, Inohara N, Nunez G. NOD1 and NOD2: signaling, host defense, and inflammatory disease. *Immunity*. 2014;41(6):898-908.

SUPPORTING INFORMATION

Additional supporting information may be found in the online version of the article at the publisher's website.

How to cite this article: Luo Z, Ji Y, Zhang D, et al. Microbial DNA enrichment promotes liver steatosis and fibrosis in the course of non-alcoholic steatohepatitis. *Acta Physiol*. 2022;00:e13827. doi:10.1111/apha.13827